well as the Centre National de la Recherche Scientifique (J.P.M., G.B.) for financial support.

Registry No. **1a**, 56183-64-3; **1b**, 102724-53-8; **1c**, 102699-27-4; **2a**, 72821-01-3; **2b**, 95552-76-4; **2c**, 50732-21-3; **2d**, 76173-65-4; **3**, 117874-61-0; **4**, 79933-17-8; **5**, 117874-62-1; **6**, 117874-63-2; **7**, 117874-64-3; **8**, 117874-65-4; **9**, 117874-66-5; **10**, 117874-67-6; **11**, 117874-68-7; **12**, 117874-69-8; **13**, 117874-70-1; **14**, 117874-71-2; **15**, 65160-85-2; **16**, 107769-94-8; **17** (diastereomer 1), 107769-96-0; **17** (diastereomer 2), 107869-72-7; **18** (diastereomer 1), 107769-95-9; **18** (diastereomer 2), 107798-25-4; **19**, 66435-40-3; **20**, 107770-00-3; **21**, 107770-01-4.

Supplementary Material Available: Tables of anisotropic thermal parameters, hydrogen atom coordinates, and additional bond distances and angles (3 pages); a table of calculated and observed structure factors (14 pages). Ordering information is given on any current masthead page. Inquiries for copies of these materials can also be directed to the corresponding authors.

Contribution from the Institut für anorganische Chemie der Universität Bern, Freiestrasse 3, CH-3000 Bern 9, Switzerland

Spin Cluster Excitations of $Ti^{2+}Mn^{2+}$ and $Mn^{2+}Ti^{2+}Mn^{2+}$ in $MgCl_2$ Studied by Site-Selective Optical Spectroscopy

Markus Herren, Stuart M. Jacobsen, and Hans U. Güdel*

Received July 6, 1988

The spin clusters Ti^{2+}–Mn^{2+} and Mn^{2+}–Ti^{2+}–Mn^{2+} were created by simultaneously doping Ti^{2+} and Mn^{2+} into single crystals of $MgCl_2$. They were studied by site-selective dye laser spectroscopy using $^4A_{1g}$, ^4E_g excitations on Mn^{2+}, and the luminescence transition observed was $^1E_g \rightarrow {}^3T_{1g}$ on Ti^{2+} (O_h single-ion notations). Exchange splittings in the electronic ground state were directly and accurately determined and the corresponding exchange parameters derived. Two types of trimers, structural isomers, could be clearly distinguished. Eleven ground-state spin levels are spectroscopically accessible, which were all observed for both trimers. The spin level structure in the trimers has the appearance of a ferromagnetic pattern. This is a direct result of the dominant antiferromagnetic Ti^{2+}–Mn^{2+} interaction, which leads to a ferromagnetic "alignment" of the Mn^{2+} spins in a classical picture. Deviations from the regular energy splitting pattern expected from a bilinear Ti^{2+}–Mn^{2+} (J) Heisenberg operator are small but significant in the spectroscopic data. They are quantitatively accounted for by including Mn^{2+}–Mn^{2+} interactions (J') as well as a biquadratic Ti^{2+}–Mn^{2+} term (j). The following parameter values were obtained: for the Ti^{2+}–Mn^{2+} dimers, $2J = -19.0$ cm^{-1} and $j = 0.5$ cm^{-1}; for the linear and bent Mn^{2+}–Ti^{2+}–Mn^{2+} trimers, $2J = -19.0$ cm^{-1}, $j = 0.5$ cm^{-1}, and $2J' = -0.1$ cm^{-1}; for triangular trimers, $2J = -19.0$ cm^{-1}, $j = 0.5$ cm^{-1}, $2J' = -2.2$ cm^{-1}, and $2J'_{exc}$ (in the ^1E_g excited state) $= -2.0$ cm^{-1}.

1. Introduction

Exchange-coupled clusters of transition-metal ions continue to fascinate the coordination chemists. There is a clear interest from the bioinorganic community, because an increasing number of active centers in metalloproteins are found to contain more than one metal atom.[1] In another area of research there is an intensive effort to design and understand new "molecular magnets", which is mainly directed toward the development of materials with novel properties.[2] Molecular systems with ferromagnetic or pseudoferromagnetic behavior appear to be of particular interest in the latter field. Antiferromagnetic pairing of electrons, on the other hand, plays an important part in some recent theoretical models developed for understanding the unusual behavior of the new family of high-T_c superconducting oxides.[3]

Dimers of magnetic ions in which the coupling is described by a Heisenberg Hamiltonian

$$\hat{H}_{ex} = -2J(\mathbf{S}_1 \cdot \mathbf{S}_2) \qquad (1)$$

show a regular spin level structure described by a Landé pattern. Trimers show a Landé splitting pattern only in a few special cases such as the equilateral triangles realized in complexes like $[Cr_3O(OAc)_6(H_2O)_3]^+$ and $[Fe_3O(SO_4)_6(H_2O)_3]^{5-}$.[4,5] In general the energy of the trimer spin states depends on two quantum numbers, and the spin-state structure is irregular. An example is provided by the linear Mn^{2+} trimers obtained by doping $CsMgBr_3$, the splitting pattern of which was recently determined.[6] Reference 6 also shows how the spin level structure evolves when the number of Mn^{2+} ions in the linear cluster increases. As expected in a semiclassical picture of nearest-neighbor antiferromagnetic coupling, the ground spin levels are $S = 0$ and $S = {}^5/_2$ for clusters with even and odd numbers of Mn^{2+} ions, respectively.

An interesting situation arises in a linear trimer ABA with dominant nearest-neighbor antiferromagnetic interaction. When A represents an ion with a large magnetic moment like Mn^{2+} ($S = {}^5/_2$) and B an ion with a smaller magnetic moment, this will lead to a pseudoferromagnetic coupling of the A spins with a resulting high-spin quantum number for the lowest energy level. The trinuclear species can then be considered as a molecular ferrimagnet. This situation has been discussed in some detail by Kahn and co-workers.[7] A molecular Mn^{2+}–Cu^{2+}–Mn^{2+} complex, as reported in ref 7, does indeed show the typical magnetic behavior of a ferromagnetically coupled complex, even though the Mn^{2+}–Cu^{2+} interactions are antiferromagnetic. The exchange energy splitting pattern is quite regular in such a situation, but not with Landé intervals. The spin levels are regularly spaced with an energy difference $\Delta E = -2J_{AB}$.

We have recently studied a very large spin cluster in which the same principles apply.[8] By doping Ti^{2+} into $MnCl_2$ we were able to determine the properties of a $Ti^{2+}(Mn^{2+})_6$ cluster, which are quite remarkable. The dominant antiferromagnetic Ti^{2+}–Mn^{2+} interaction leads to a pseudoferromagnetic coupling of all the six Mn^{2+} spins and thus very large spin quantum numbers of the lowest energy cluster levels. The ground level is $|S_a\, S\rangle = |15\ 14\rangle$, where S_a is the sum of all the Mn^{2+} spins and S the total cluster spin.

In the present study we report high-resolution spectroscopic results on Ti^{2+}–Mn^{2+} dimers and two types of Mn^{2+}–Ti^{2+}–Mn^{2+} trimers obtained by doping both Ti^{2+} and Mn^{2+} in $MgCl_2$. The

* To whom correspondence should be addressed.

(1) Solomon, E. I.; Wilcox, D. E. *Magneto-Structural Correlations in Exchange Coupled Systems*; Willett, R. D., Gatteschi, D., Kahn, O., Eds.; Nato ASI Series; Reidel: Dordrecht, The Netherlands, 1985; Series C, Vol. 140.
(2) Kahn, O. *Angew. Chem., Int. Ed. Engl.* **1985**, *24*, 834 and references therein.
(3) De Jongh, L. J. *Solid State Commun.* **1988**, *65*, 963.
(4) Ferguson, J.; Güdel, H. U. *Aust. J. Chem.* **1973**, *26*, 513.
(5) Furrer, A.; Güdel, H. U. *Helv. Phys. Acta* **1977**, *50*, 439.
(6) Falk, U.; Furrer, A.; Güdel, H. U.; Kjems, J. K. *Phys. Rev. B* **1987**, *35*, 4888.
(7) Pei, Y.; Journaux, Y.; Kahn, O. *Inorg. Chem.* **1988**, *27*, 399.
(8) Jacobsen, S. M.; Güdel, H. U.; Smith, W. E. *Inorg. Chem.* **1987**, *26*, 2001.

0020-1669/89/1328-0504$01.50/0

spectral resolution is increased by an order of magnitude compared with Ti^{2+}-doped $MnCl_2$, and all of the transitions to the ground-state spin levels are fully resolved. The sharpness of the luminescence lines is due to the fact that the underlying electronic transitions $^1E_g \rightarrow {}^3A_{2g}$, ^3E_g (D_{3d} notation) take place within the same high-spin configuration; they are thus essentially spin-flip transitions. The "picket-fence" spin-level structure expected for the trimers can thus actually be seen for the first time (see Figure 4). Slight deviations from the regular pattern are accurately determined and interpreted. As a result of the simplicity of the crystal structure there are only three different types (isomers) of Mn^{2+}–Ti^{2+}–Mn^{2+} trimers in this lattice: linear and bent by 120 and 60°, respectively. A tunable dye laser allows their selective excitation and, as a result, a detailed study of their individual properties.

2. Experimental Section

(a) Crystal Preparation. All the experiments reported here were carried out on samples from the same crystal boule. It was synthesized as follows. First a crystal of $MgCl_2$ containing only Ti^{2+} was grown by the Bridgman technique by using an in situ reaction to generate the titanium ions as described in ref 9. It was then combined with an appropriate amount of anhydrous $MnCl_2$ in a silica ampule, and this mixture was regrown by the Bridgman method to produce the co-doped crystal. The Ti^{2+} and Mn^{2+} concentrations were determined colorimetrically and by atomic absorption, respectively: Ti^{2+}, 0.3%; Mn^{2+}, 5%.

(b) Spectroscopic Measurements. $MgCl_2$ is a layer lattice with the $CdCl_2$ structure;[10] single crystals cleave readily perpendicular to the c axis, and all spectroscopic measurements were taken with light propagating along this axis. Absorption experiments in the near-IR were performed as follows. Light from a 150-W quartz-halogen lamp was dispersed by a 0.75-m Spex 1702 monochromator. After passing through a tuning-fork chopper (Bulova), the near-IR radiation was focussed on the sample and detected with a cooled (77 K) germanium photodetector (Applied Detector Corp., Model 403L). The signal was recorded by using a PAR 186A lock-in amplifier and subsequently transformed from transmission to absorbance by a computer. Sample cooling was achieved with an Air Products Displex closed-cycle cryogenic refrigerator.

Site-selective luminescence spectra were recorded by using a LSI DCM-2 grazing incidence dye laser (with stilbene in methanol as dye) pumped with a PRA LN-250 nitrogen laser. The luminescence was dispersed by the Spex 1702 monochromator and detected with the cooled germanium photodetector. In these experiments cooling was achieved with helium gas by mounting the samples in silica flow tubes.

In all the spectroscopic measurements, data acquisition and monochromator control were performed by a Tektronix 4052A microcomputer.

3. Exchange Interactions

3.1. Ground State. In octahedral symmetry Ti^{2+} has a $^3T_{1g}$ ground state. In $MgCl_2$ the site symmetry is D_{3d}, and the $^3T_{1g}$ state is split by the trigonal potential by approximately 750 cm^{-1}, with the trigonal $^3A_{2g}$ component lying lower.[9] Orbital angular momentum is thus almost completely quenched in the ground state. Since Mn^{2+} has a pure spin-only ground state, the Ti^{2+}–Mn^{2+} interaction is adequately described by the Heisenberg Hamiltonian (eq 1). For antiferromagnetic coupling and $S_{Ti} = 1$, $S_{Mn} = {}^5/_2$ we get the dimer splitting pattern shown schematically in Figure 1. Inclusion of a biquadratic term leads to the Hamiltonian

$$\hat{H}_{dimer} = -2J(\mathbf{S}_{Ti}\cdot\mathbf{S}_{Mn}) - j(\mathbf{S}_{Ti}\cdot\mathbf{S}_{Mn})^2 \quad (2)$$

with the eigenvalues

$$E(S) = -J[S(S+1) - S_{Ti}(S_{Ti}+1) - S_{Mn}(S_{Mn}+1)] - 1/4j[S(S+1) - S_{Ti}(S_{Ti}+1) - S_{Mn}(S_{Mn}+1)]^2 \quad (3)$$

where S is the total dimer spin quantum number. Inserting S_{Ti} and S_{Mn}, we get the following S dependence of the dimer energy levels

$$E(S) = \left(-J + \frac{43}{8}j\right)S(S+1) - \frac{j}{4}\cdot S^2(S+1)^2 + \text{constant} \quad (4)$$

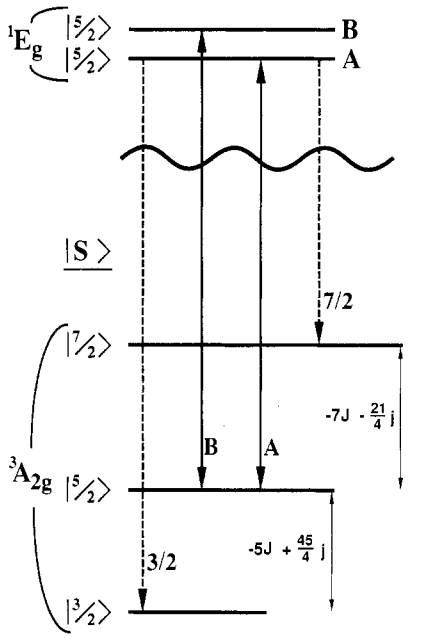

Figure 1. Energy splittings of the ground state and the emitting state for Ti^{2+}–Mn^{2+} dimers in $MgCl_2$. The spin labels refer to the total dimer spin. Energy differences in the ground state refer to eq 2. The transition labels are used in the text and in Figure 4. The degeneracies of the levels are expressed by the lengths of the corresponding lines.

In a trimer the exchange interaction can to a good approximation be built up of pairwise interactions. Including biquadratic terms it is given by

$$\hat{H}_{Trimer} = -2J(\mathbf{S}_{Ti}\cdot\mathbf{S}_{Mn1} + \mathbf{S}_{Ti}\cdot\mathbf{S}_{Mn2}) - 2J'(\mathbf{S}_{Mn1}\cdot\mathbf{S}_{Mn2}) - j[(\mathbf{S}_{Ti}\cdot\mathbf{S}_{Mn1})^2 + (\mathbf{S}_{Ti}\cdot\mathbf{S}_{Mn2})^2] \quad (5)$$

In this expression we have omitted the biquadratic Mn1–Mn2 term, which is expected to be negligible. Using the techniques in ref 11, we derive the following expression for the eigenvalues of eq 5 (see Appendix):

$$E(S',S) = \left(-J + \frac{j}{4}\right)[S(S+1) - S'(S'+1) - 2] - J'[S'(S'+1) - {}^{35}/_2] - 20(14^{1/2})jM_{TiMn}(S',S) \quad (6)$$

with

$$M_{TiMn}(S',S) = (-1)^S(2S+1)\begin{Bmatrix} S' & S' & 2 \\ {}^5/_2 & {}^5/_2 & {}^5/_2 \end{Bmatrix}\begin{Bmatrix} S' & S' & 2 \\ 1 & 1 & S \end{Bmatrix} \quad (7)$$

The two quantum numbers S' and S required to label the trimer levels are based on the following coupling scheme:

$$\mathbf{S}' = \mathbf{S}_{Mn1} + \mathbf{S}_{Mn2}$$
$$\mathbf{S} = \mathbf{S}' + \mathbf{S}_{Ti} \quad (8)$$

with $S_{Mn} = {}^5/_2$ and $S_{Ti} = 1$, S' can take values from 0 to 5, and S from $|S'-1|$ to $S'+1$. For the simple but physically relevant case that $J = J_{Ti-Mn}$ is dominant and J' and j can be neglected, eq 6 leads to the regular energy splitting pattern shown in Figure 2. This ladder-type spin level structure with an energy interval of $-2J$ between neighboring levels is very typical for clusters of this type. There is a central, highly degenerate level containing all the five trimer states with $S' = S$. To higher and lower energy, respectively, we have the $S = S'+1$ and $S = S'-1$ wings of levels.

Deviations from the regular energy pattern in Figure 2 can be caused by biquadratic interactions as well as Mn1–Mn2 interactions (j and J' in eq 5 and 6). The effect of j is essentially that of a depression of the levels with high S quantum numbers. As a consequence the energy intervals will tend to decrease with increasing energy, and the central $|S' = S\rangle$ levels will split. The

(9) Jacobsen, S. M.; Güdel, H. U.; Daul, C. A. *J. Am. Chem. Soc.* **1988**, *110*, 7610.
(10) Wyckoff, R. W. G. *Crystal Structures*, 2nd ed.; Interscience: New York, 1965; Vol. 1, p 270.
(11) Griffith, J. S. *Struct. Bonding (Berlin)* **1972**, *10*, 87.

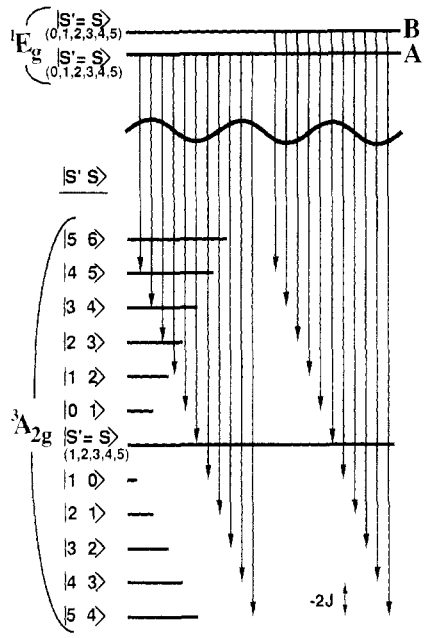

Figure 2. Energy splittings of the ground state and the emitting state for Mn^{2+}–Ti^{2+}–Mn^{2+} trimers in $MgCl_2$. S' is the spin of the Mn^{2+} pair, and S is the total trimer spin. The regular energy splitting is for a situation in which all but the bilinear Ti^{2+}–Mn^{2+} exchange interactions J are zero. The degeneracies of the levels are expressed by the lengths of the corresponding lines.

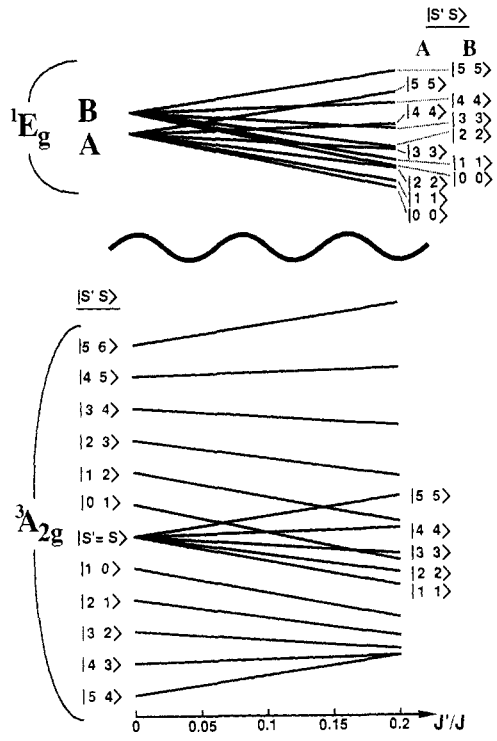

Figure 3. Effect of J' (Mn^{2+}–Mn^{2+} interactions, eq 5) on the exchange splitting pattern of Figure 2. J' is assumed to be equal in the ground and emitting states.

effect of an antiferromagnetic J' is shown in Figure 3. The ground-state levels with high S quantum numbers are raised in energy, and part of the degeneracy of the central levels with $S' = S$ is lifted, resulting in a Landê splitting pattern according to

$$E(S' = S) = -J'[S(S + 1) - 35/2] \quad (9)$$

The combined effect of j and J' is thus most pronounced for the central band, affecting both its position and shape. The spectra do indeed show this.

3.2. Excited State. The luminescent state of Ti^{2+} in $MgCl_2$ is ^1E_g.[12] It is degenerate in D_{3d}, but in the dimers and trimers

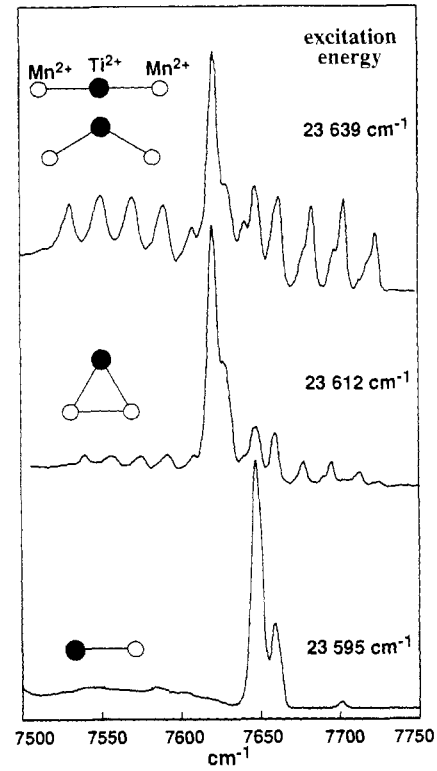

Figure 4. Selectively excited emission spectra at 5 K for Ti^{2+}–Mn^{2+} dimers and Mn^{2+}–Ti^{2+}–Mn^{2+} trimers in $MgCl_2$. Ordinate scales are arbitrary and unrelated. Excitation energies are given on the right-hand side.

this degeneracy is lifted, because the 3-fold rotation axis at the Ti^{2+} site is lost. As a consequence the ^1E_g state is split into two orbital components ^1A and ^1B. We arbitrarily label the lower and higher energy components A and B, respectively.

There are no exchange interactions in a Ti^{2+}–Mn^{2+} dimer with Ti^{2+} in these excited states, because Ti^{2+} has no magnetic moment. There is thus no further splitting, and the two emitting dimer states both have $S = 5/2$, because $S_{Mn} = 5/2$. For transitions to the ground-state multiplet we have the selection rule $\Delta S = 0$, if the intensity arises by an exchange mechanism.[13] This is the case, as will be shown, and the transitions from the two $S = 5/2$ emitting states to the $S = 5/2$ ground level dominates the dimer emission spectrum. Transitions with $\Delta S = \pm 1$ are possible by a single-ion mechanism. They are 2 orders of magnitude weaker than the exchange-induced transitions in our case. The spectroscopic situation is depicted in Figure 1.

In a trimer with Ti^{2+} in its first excited state, there remains the Mn1–Mn2 interaction, i.e. the J' term in eq 5. The excited state splitting is thus given by an equation exactly analogous to eq 9:

$$E(S' = S)_{exc} = -J'_{exc}[S(S + 1) - 35/2] \quad (10)$$

The resulting Landê splitting is also shown in Figure 3.

For an exchange intensity mechanism we have the selection rule $\Delta S = 0$. Transitions from both excited states A and B to all but one of the ground-state levels are thus allowed (see Figure 2). And, as we will show, they can all be observed. For $J' \neq 0$ there is the additional selection rule $\Delta S' = 0$ for exchange-induced intensity. Since in our trimers J' is very close to zero, we expect it to be relaxed.

4. Results

Details of the site-selective spectroscopy in these doubly doped $MgCl_2$ crystals are described and discussed elsewhere.[14] Here

(12) Jacobsen, S. M.; Smith, W. E.; Reber, C.; Güdel, H. U. *J. Chem. Phys.* **1986**, *84*, 5205.
(13) Ferguson, J.; Guggenheim, H. J.; Tanabe, Y. *J. Phys. Soc. Jpn.* **1966**, *21*, 692.
(14) Herren, M.; Jacobsen, S. M.; Güdel, H. U. *J. Chem. Phys.*, in press.

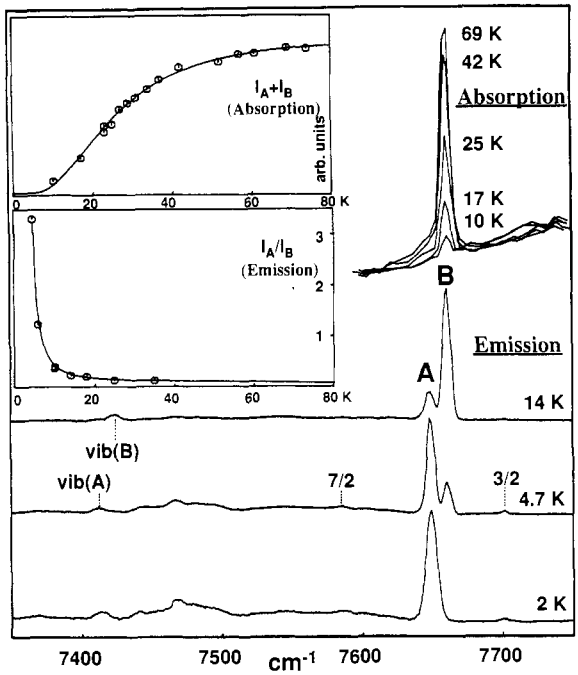

Figure 5. $Ti^{2+}Mn^{2+}$ dimer absorption and emission spectra (excitation at 23 595 cm^{-1}) as a function of temperature. The transitions are labeled according to Figure 1. The inserts show the temperature dependence of the intensities with the corresponding calculated curves referred to in section 5.2.

we present those spectroscopic results that determine the energy splittings in the ground and first excited state for both the dimer and the trimers.

Figure 4 shows the $^1E_g \rightarrow {}^3A_{2g}$ part of the 5 K emission spectra of selectively excited Ti^{2+}–Mn^{2+} dimers and the various types of Mn^{2+}–Ti^{2+}–Mn^{2+} trimers. The lifetime of the dimer emission at 5 K is 1.7 ms.[14] There are three geometrical isomers of such trimers in this crystal lattice. Each metal ion has six equivalent nearest neighbors arranged hexagonally in the *a,b* plane. We thus have trimers with 60° (*triangular*), 120° (*bent*), and 180° (*linear*) angles at the Ti^{2+}. With the Ti^{2+} and Mn^{2+} contents in our crystal and assuming a statistical distribution, we calculate the following abundances (in percent of Ti^{2+}): 19.4 for dimers and 0.9 for triangular, 0.9 for bent, and 0.4 for linear trimers, respectively. Whereas the triangular trimer has a distinctly different splitting pattern from the bent and the linear trimers, the latter two have nondistinguishable splittings and thus coincide in the spectrum.

Figure 5 shows the coincidence of the two dimer lines A and B (cf. Figure 1) in absorption and emission. It also shows that both lines are hot lines in absorption, as expected from Figure 1. In emission the line A is cold, whereas B is hot. The energy difference of 12.5 cm^{-1} between A and B is thus the orbital splitting in the excited state. The very weak $\Delta S = \pm 1$ lines are also indicated in the emission spectrum of Figure 5. The vibrational sideband structure is mainly associated with the cold band A. Only the bands designated vib(A) and vib(B), separated by 236.5 cm^{-1} from their origins, have comparable intensity in both the A and B spectra. This 236.5-cm^{-1} mode is assigned as a totally symmetric vibration.

Figure 6 shows the emission spectrum of linear and bent Mn^{2+}–Ti^{2+}–Mn^{2+} trimers as a function of temperature. It is slightly contaminated by the dimer spectrum, because the spectroscopic selectivity of excitation is not perfect. The dimer bands are indicated. The spectrum shows very nicely and impressively the "picket-fence" behavior expected for such a trimer. A large number of individual trimer bands are observed, and the qualitative agreement with the splitting pattern predicted in Figure 2 makes an assignment straightforward. There is clearly a cold and a hot set of bands, with the same splitting patterns in both sets, and with set B (hot) displaced by 12.5 cm^{-1} to higher energy with respect to set A (cold). This shift is exactly analogous to the energy difference between the A and B lines in the dimer spectrum.

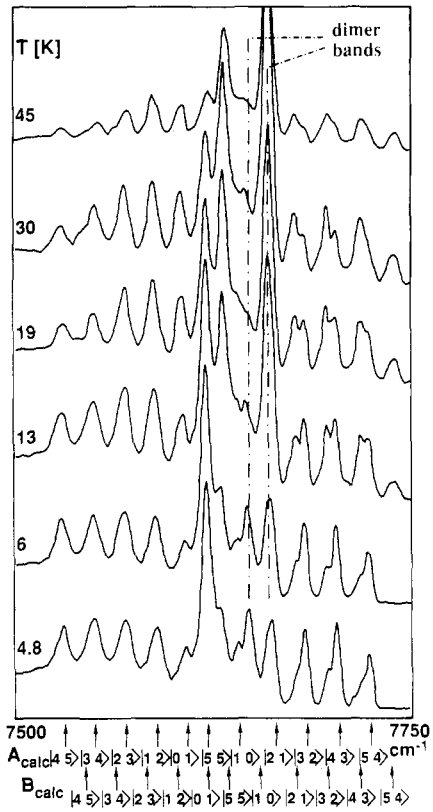

Figure 6. Emission spectra, excited at 23 639 cm^{-1}, of linear and 120° bent Mn^{2+}–Ti^{2+}–Mn^{2+} trimers as a function of temperature. Two superimposed dimer bands are indicated. Assignments in terms of $|S'S\rangle$ of the cold (A) and hot (B) trimer bands and the calculated positions (J = −9.5 cm^{-1}, J' = −0.05 cm^{-1}, J'_{exc} = 0, j = 0.5 cm^{-1}) are given at the bottom.

It is due to an orbital splitting of the ^1E_g emitting state. The observed energy intervals between neighboring bands are not exactly constant. This deviation is most noticeable in the region around the most central line. An analysis of these intervals and the intensity distribution will be provided in section 5.3.

Figure 7 shows the emission spectrum of the triangular $Ti^{2+}(Mn^{2+})_2$ trimers as a function of temperature. It is qualitatively similar to the spectrum in Figure 6, and accordingly, the assignment of the bands is quite analogous. The total energy spread and the individual energy intervals are slightly but significantly smaller than for the trimers of Figure 6. In addition, the central line is much more prominent in intensity. All these features will be analyzed and discussed in section 5.3.

5. Analysis and Discussion

5.1. Excitation and Energy Transfer. As shown in detail in ref 14, the selective excitation of the various magnetic clusters, which is of course an essential condition for the present work, is achieved by exciting into the $^4A_{1g}$, ^4E_g bands of Mn^{2+} centered around 23 600 cm^{-1}. These Mn^{2+} excitations, being pure spin-flips in the octahedral approximation, are extremely sharp. As a result of very slight differences of interelectron repulsion parameters, corresponding excitations have slightly different energies in the various clusters. These differences are on the order of 10–30 cm^{-1} (Figure 4), which is on the order of one-tenth of a percent of the total excitation energy. But the natural widths of the absorption bands are even smaller than these differences, and site-selective excitation is achieved by tuning a dye laser to the appropriate energy.

It is of course important for the selectivity to work that Ti^{2+} has no absorptions around 23 600 cm^{-1}. This is the case, as was shown by the absorption spectrum of Ti^{2+} in $MgCl_2$.[15] In our dimers and trimers we thus excite the Mn^{2+} ions and observe luminescence from the Ti^{2+} ions. One can say that part of the

(15) Wilson, D. R.; Smith, W. E. *Inorg. Chem.* **1986**, *25*, 898.

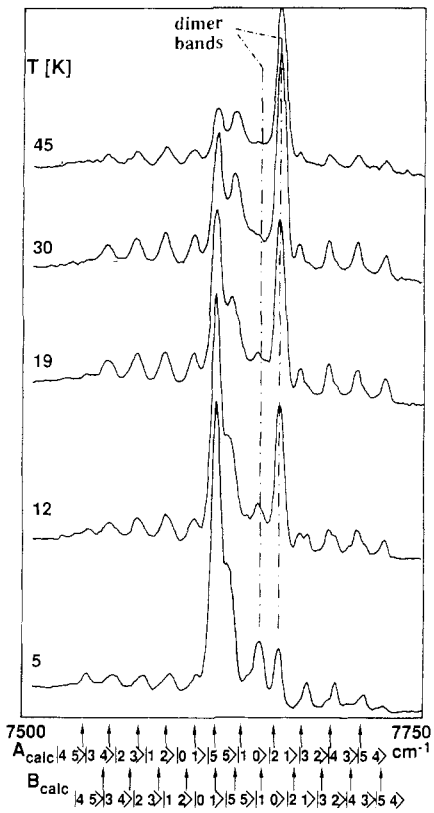

Figure 7. Emission spectra as in Figure 6, but for the 60° bent (triangular) Mn^{2+}–Ti^{2+}–Mn^{2+} clusters, excited at 23 612 cm^{-1}. Calculated positions with $J = -9.5$ cm^{-1}, $J' = -1.1$ cm^{-1}, $J'_{exc} = -1.0$ cm^{-1}, and $j = 0.5$ cm^{-1}.

excitation energy is transferred from Mn^{2+} to Ti^{2+}. This is a view which is favored by many physicists: individual chromophores that are weakly coupled by exchange interactions. Nonradiative energy transfer from the donor (Mn^{2+}) to the acceptor (Ti^{2+}) then takes place through an exchange mechanism.[16] An important factor in this model is the spectral overlap between the emission of the donor and an absorption of the acceptor. This is very favorable in our case, because the $^4T_{1g} \rightarrow {}^6A_{1g}$ Mn^{2+} emission, peaking at 15 400 cm^{-1} at 10 K, almost ideally overlaps with the $^3T_{1g} \rightarrow {}^3T_{2g}$ Ti^{2+} absorption, peaking at 16 130 cm^{-1} at 10 K.

Chemists tend to view the situation differently. The clusters are considered as the relevant units in the crystal, which determine the magnetic and spectroscopic properties. Electronic excitations are thus a priori delocalized, because the wave functions are delocalized. This view was implicit in the theoretical treatment of cluster interactions in section 3.

5.2. Dimer Transitions. The assignment of the lines A and B in Figure 5 to the transitions in Figure 1, as indicated by the full arrows, is straightforward. The coincidence in absorption and luminescence identifies the lines as belonging to the same center in the crystal. The dominance in intensity of the A and B origins clearly demonstrates that most of the intensity in this spectral range is exchange induced. This is supported by the lifetime of the emission of 1.7 ms at 5 K, which is 2 orders of magnitude shorter than the lifetime of Ti^{2+} single ions in this host. The different sideband structures of the A and B bands reflect their different orbital character. Transition B, corrected for Boltzmann factors, is more intense than transition A by a factor of 14. It appears that the orbital composition of state B is more favorable for inducing intensity to the ground state. The temperature dependence of line B in emission is in excellent agreement with its energy separation of 12.5 cm^{-1} from line A, as shown in the lower insert of Figure 5.

The temperature dependence of the hot absorption band (insert in Figure 5) corresponds to the Boltzmann population of the $S = {}^5/_2$ ground level. From a least-squares fit we estimate values of 36 and 50.5 cm^{-1} for the $|{}^3/_2\rangle - |{}^5/_2\rangle$ and $|{}^5/_2\rangle - |{}^7/_2\rangle$ energy separations, respectively. This is only a rough estimate, since the absorption intensities are not accurate. The emission spectrum allows a much more precise determination of this energy difference. The weak cold line at 7701 cm^{-1} could be shown to have the same excitation spectrum and temperature dependence as the line A. It thus belongs to the cold dimer spectrum, and we can safely assign it to the $^3/_2$ transition (Figures 1 and 5). The resulting energy difference between the $|{}^5/_2\rangle$ and $|{}^3/_2\rangle$ ground levels is thus 53 cm^{-1}. Another weak and sharp cold feature in the emission spectrum, occurring 63.5 cm^{-1} below the $^5/_2$ line, is assigned to the $^7/_2$ transition (Figure 5). Both J and j can now be determined by using eq 4:

$$2J_{dimer} = -19.0 \text{ cm}^{-1}$$

$$j_{dimer} = 0.5 \text{ cm}^{-1} \qquad (11)$$

5.3. Trimer Transitions. The spectra in Figures 6 and 7 are absolutely unique in optical spectroscopy. Qualitatively they look more like hyperfine split EPR spectra or rotational spectra than electronic spectra. At first sight one might suspect a vibrational progression of an electronic transition. But this is clearly ruled out by both the intensity distribution and the energy intervals of approximately 20 cm^{-1}. One is forced to the conclusion that the observed regular intervals between adjacent lines are due to a regular splitting of an electronic state. As developed in section 3, such a splitting is expected for an exchange-coupled Mn^{2+}–Ti^{2+}–Mn^{2+} trimer with dominant Ti^{2+}–Mn^{2+} interaction. A dominance of the Ti^{2+}–Mn^{2+} interaction J is naturally given in the linear and bent trimers. But even in the triangular trimer with one Mn^{2+}–Mn^{2+} nearest-neighbor contact the Mn^{2+}–Mn^{2+} interaction J' is an order of magnitude smaller than J, and the pattern remains fairly regular.

It is thus obvious that the spectra in Figures 6 and 7 are to be assigned to trimer transitions and splitting patterns as shown in Figure 2. The number of observed lines in both the cold (A) and hot (B) sets is 11, i.e. exactly that predicted by the $\Delta S = 0$ selection rule. The highest energy ground level $|5\ 6\rangle$ is spectroscopically unaccessible, because there is no S=6 level in the emitting states. With this assignment we get an immediate estimate of J. The observed energy intervals of roughly 20 cm^{-1} correspond to $-2J$. This is in very good agreement with the $2J = -19$ cm^{-1} value determined for the dimers (section 5.2).

We now proceed to analyze the deviations from the regular pattern and the differences between the various trimers. The theoretical model has been accordingly developed in section 3. It is obvious that the spectra in Figures 6 and 7 belong to different isomers. We have several reasons for assigning the spectrum in Figure 7 to triangular clusters and the spectrum in Figure 6 to a superposition of bent and linear clusters. The reduction of 22 cm^{-1} in the total energy spread of the spectrum in Figure 7 compared to that in Figure 6 is a result of the nonzero J' in the triangular clusters. The intensity dominance of the central line in Figure 7 is another consequence of this Mn^{2+}–Mn^{2+} interaction, because the $\Delta S' = 0$ selection rule has more meaning here.

The deviation of the central line from the regular energy pattern is more pronounced in Figure 7, another result of the bigger J' (cf. Figure 3).

For both spectra the observed energy intervals were fitted with the eigenvalues given in eq 6 and 10. Excellent fits were obtained with J and j held fixed at the dimer values and J' and J'_{exc} as variable parameters. The results obtained for the following parameter sets are included in Figures 6 and 7.

	bent and linear	triangular
$2J$, cm^{-1}	−19.0	−19.0
j, cm^{-1}	0.5	0.5
$2J'$, cm^{-1}	−0.1	−2.2
$2J'_{exc}$, cm^{-1}	0	−2.0

We notice that the same Ti^{2+}–Mn^{2+} interaction parameters describe the observed splittings in the dimers and both types of

(16) Dexter, D. L. *J. Chem. Phys.* **1953**, *21*, 836.

trimers. This internal consistency is gratifying, and it can be taken as another confirmation that all the patterns have been properly assigned. The difference between the bent/linear trimers and the triangular trimers lies in the J' values, i.e. the Mn^{2+}–Mn^{2+} interactions, which are quite significant in the triangular case but rather unimportant for the other trimers. This is, of course, expected since nearest-neighbor Mn^{2+}–Mn^{2+} contacts only occur in the triangle. And the parameter value of $2J' = -2.0$ cm^{-1} found in our analysis is close to the corresponding value $2J = -1.4$ cm^{-1} found for nearest-neighbor Mn^{2+}–Mn^{2+} dimers in the similar lattice $CdCl_2$.[17]

6. Conclusions

We have been able to directly observe and measure the regular energy splitting pattern that results from exchange interactions in trimers like Mn^{2+}–Ti^{2+}–Mn^{2+}. Besides the regular energy intervals, the spin-level structure is characterized by its *apparent ferromagnetic* ordering of the levels. This does not mean, however, that there are any truly ferromagnetic interactions in the cluster. Both J and J' are antiferromagnetic. The level ordering is a result of the dominance of the Ti^{2+}–Mn^{2+} interactions J compared to the Mn^{2+}–Mn^{2+} interactions J'. In a classical picture the most stable configuration thus corresponds to a parallel alignment of the two Mn^{2+} moments. The apparent ferromagnetic ordering of energy levels follows from the fact that the Mn^{2+} magnetic moments ($S_{Mn} = {}^5/_2$) are larger than the Ti^{2+} ($S_{Ti} = 1$) magnetic moment.

Due to its *high selectivity* as well as *sensitivity* the spectroscopic technique is superior to bulk techniques for the determination of such cluster properties. Deviations from the regular splitting pattern are readily observed, and thus the weaker effects like biquadratic exchange and Mn^{2+}–Mn^{2+} interactions become directly accessible to experiment. Site-selective spectroscopy allows the determination of individual cluster properties in the same crystal and thus a comparison under well-defined conditions.

Acknowledgment. We are grateful to Christian Reber for many useful discussions. This work was financially supported by the Swiss National Science Foundation.

Appendix

With the coupling scheme

$$\mathbf{S}' = \mathbf{S}_{Mn1} + \mathbf{S}_{Mn2}$$
$$\mathbf{S} = \mathbf{S}' + \mathbf{S}_{Ti} \qquad \text{(A1)} = \text{(8)}$$

we use the functions $|(S_{Mn1}\, S_{Mn2})\, S'\, S_{Ti}\, S\rangle$ or, abbreviated $|S'\, S\rangle$, as our basis for the energy calculation. The matrix of the operator

$$\hat{H}_{Trimer} = -2J(\mathbf{S}_{Ti}\cdot\mathbf{S}_{Mn1} + \mathbf{S}_{Ti}\cdot\mathbf{S}_{Mn2}) - 2J'(\mathbf{S}_{Mn1}\cdot\mathbf{S}_{Mn2}) - j[(\mathbf{S}_{Ti}\cdot\mathbf{S}_{Mn1})^2 + (\mathbf{S}_{Ti}\cdot\mathbf{S}_{Mn2})^2] \quad \text{(A2)} = \text{(5)}$$

is not diagonal in this basis. Off-diagonal elements arise from the biquadratic term between functions $|S'\, S\rangle$ and $|S'\, -2\, S\rangle$. Energy differences between these states are large (cf. Figure 2), and we can neglect the off-diagonal elements. Considering only diagonal elements, we can derive the eigenvalues of the three terms in eq A2 separately:

$$E(S',S) = -J[S(S+1) - S'(S'+1) - 2] - J'[S'(S'+1) - {}^{35}/_2] + j\cdot X \qquad \text{(A3)}$$

To evaluate $j\cdot X$ we use the procedure of ref 11. Inclusion of the biquadratic exchange parameter j also leads to a correction of the bilinear term:

$$j\cdot X = \frac{j}{4}[S(S+1) - S'(S'+1) - 2] + E_{biq}(S',S) \quad \text{(A4)}$$

The remaining biquadratic term $E_{biq}(S',S)$ can be expressed as[11]

$$E_{biq}(S',S) = 2[a_2(\mathrm{Ti,Mn})]M_{TiMn}(S',S) \qquad \text{(A5)}$$

with the matrix element

$$M_{TiMn}(S',S) = (-1)^S(2S+1)\begin{Bmatrix} S' & S' & 2 \\ {}^5/_2 & {}^5/_2 & {}^5/_2 \end{Bmatrix}\begin{Bmatrix} S' & S' & 2 \\ 1 & 1 & S \end{Bmatrix} \qquad \text{(A6)} = \text{(7)}$$

where the material in braces represents $6-j$ symbols, and the coefficient is

$$a_2(\mathrm{Ti,Mn}) = -\frac{1}{6}j[(2S_{Ti}-1)(2S_{Ti}+3)(2S_{Mn}-1)(2S_{Mn}+3)(S_{Ti}+1)(2S_{Ti}+1)(S_{Mn}+1)(2S_{Mn}+1)S_{Ti}S_{Mn}]^{1/2} \quad \text{(A7)}$$

Inserting $S_{Ti} = 1$ and $S_{Mn} = {}^5/_2$ we get

$$a_2(\mathrm{Ti,Mn}) = -10(14^{1/2})j \qquad \text{(A8)}$$

Combining eq A3–A8, we get the final expression:

$$E(S',S) = \left(-J + \frac{j}{4}\right)[S(S+1) - S'(S'+1) - 2] - J'[S'(S'+1) - {}^{35}/_2] - 20(14^{1/2})jM_{TiMn}(S',S) \quad \text{(A9)} = \text{(6)}$$

with $M_{TiMn}(S',S)$ as given in eq A6.

Registry No. Ti^{2+}, 15969-58-1; Mn^{2+}, 16397-91-4; $MgCl_2$, 7786-30-3.

(17) McCarthy, P. J.; Güdel, H. U. *Inorg. Chem.* **1986**, *25*, 838.

Contribution from the Department of Chemistry and Materials Science Center, Cornell University, Ithaca, New York 14853-1301

Deformations in Mixed-Valence Cu(I)–Cu(II) Polymers

Paul Sherwood and Roald Hoffmann*

Received April 14, 1988

Some remarkable $Cu_2X_2^-$ (X = Br, Cl) chains recently synthesized by Willett are the impetus to this work. These present one-dimensional extended arrays with well-defined localized perturbations from a basic edge-sharing tetrahedral geometry. We address the electronic structure of these mixed-valence Cu(I)–Cu(II) systems by a construction that begins from a $CuCl_4^{2-}$ ion of S_4 symmetry, progressing through a $Cu_2Cl_6^{3-}$ dimer to the $Cu_2Cl_4^-$ polymers. The energy changes that result from various symmetry-lowering twists and bond length deformations are small, but they are understandable in terms of an orbital overlap and symmetry analysis. Our calculations suggest that the polymer ground states are likely to be magnetic insulating ones and their structures strongly influenced by crystal-packing factors.

Quasi-one-dimensional materials have had a special place in experimental and theoretical solid-state chemistry for many years.[1] While they provide simple models of use in the teaching and understanding of solid-state electronic structure, their low di-

0020-1669/89/1328-0509$01.50/0